Isotopic equilibrium constraints on CO_2 dissolution and carbon isotopic reversal in a thermogenic coalbed gas system associated with the Zhuzang syncline, Guizhou, China

Xiangrui Chen[1], Yunpeng Wang[1 *], Mingxin Tao[2], Zheng Zhou[3], Meng Wei[4]

[1] *State Key Laboratory of Deep Earth Processes and Resources, Guangzhou Institute of Geochemistry, Chinese Academy of Sciences, Guangzhou 510640, China*

[2] *Faculty of Geographical Science, Beijing Normal University, Beijing 100875, China*

[3] *Lancaster Environment Centre, Lancaster University, Lancaster LA1 4YQ, UK*

[4] *Sinopec Chongqing Shale Gas Co., Ltd, Chongqing 408400, China*

*Corresponding author. Email: wangyp@gig.ac.cn

Abstract

Natural gas is a vital energy resource. The isotopic composition of natural gas plays a critical role in understanding its origin, thermal maturity, and secondary alteration. Both kinetic and equilibrium isotopic fractionations have been observed in various natural gas systems. However, the dominant mechanism (either equilibrium or kinetic) that controls the isotopic compositions of the primary natural gas is still unclear. Coalbed gas (CBG), formed and stored in situ coalbeds, is an ideal natural gas for studying this key issue. We collected CBG and coproduced water samples from the Zhuzang syncline in China. This study shows that the CBG is an over-mature thermogenic gas formed during the Yanshanian orogeny. The CH_4-C_2H_6-CO_2 system was likely near carbon

isotope equilibrium during the CBG formation. However, later alterations, such as meteoric water recharge, CO_2 dissolution, and CBG recovery led to obvious isotopic disequilibrium of the CH_4-C_2H_6-CO_2-DIC (dissolved inorganic carbon) system. Carbon isotope reversals ($\delta^{13}C_{CH4} > \delta^{13}C_{C2H6}$) were observed in the CBG samples, resulting from decreasing $\delta^{13}C_{C2H6}$ values after CBG formation. Based on isotopic equilibrium, the $\delta^{13}C$ values of the primary ethane were estimated. Some hypotheses often used to explain isotope reversals in natural gas cannot explain the isotope reversals of the CBG samples. We propose that the CBG recovery process led to more negative $\delta^{13}C_{C2H6}$ and thus $\delta^{13}C_{CH4} > \delta^{13}C_{C2H6}$. Model-estimated 53-99% CO_2 generated during thermogenic or microbial CBG formation has dissolved into coalbed water to become DIC. Hence, dissolution trapping is an important mechanism for CO_2 storage in coalbeds over geological timescales. This study implies that isotopic equilibrium fractionation plays a vital role in understanding the primary geochemical composition and secondary alteration of CBG.

Keywords: Coalbed gas; Coproduced water; Isotopic equilibrium; Isotope reversal; CO_2 dissolution

1. Introduction

Natural gas is a vital energy resource and plays an indispensable role in global energy systems. Understanding its formation and evolution processes is critical for formulating effective strategies for exploration and production.

The isotopic composition of natural gas is critical for understanding its formation and evolution. Previous studies commonly assumed that kinetic processes and thus kinetic fractionations largely control the isotopic composition of natural gas (Whiticar et al., 1986; Tang et al., 2000; Turner et al., 2021). Based on kinetic isotopic effects, empirical isotopic indicators for identifying the origin and secondary alteration of natural gas have been summarized and applied (Whiticar et al., 1986; Chung et al., 1988; Milkov and Etiope, 2018; Liu et al., 2019). However, over the past 20 years, both kinetic and equilibrium isotopic fractionations have been observed in microbial, thermogenic and abiotic natural gas systems (Thiagarajan et al., 2020; Turner et al., 2021; Chen et al., 2019, 2023a). Whether or not the equilibrium mechanism controls the isotopic compositions of the primary natural gas is still unclear. It is one of the most important bases for using isotope indicators to reliably identify the origins, formation pathways, degree of thermal evolution, and secondary alterations of natural gas (Dai et al., 2016, 2018; Liu et al., 2019; Thiagarajan et al., 2020; Chen et al., 2023a). It is challenging to study this crucial issue because the isotopic composition of the primary natural gas has likely changed since its formation. Compared with other natural gas, coalbed gas (CBG), formed and stored in situ coalbeds, seems more suitable to investigate this question due to its limited post-genetic migration (Tao et al., 2021).

Currently, the most comprehensive geochemical indicators for distinguishing the origin, thermal maturity, and secondary alteration of CBG are the revised genetic diagrams of natural gas ($C_{CH4}/(C_{C2H6}+C_{C3H8})$ versus $\delta^{13}C_{CH4}$, $\delta^{13}C_{CH4}$ versus δD_{CH4}, and $\delta^{13}C_{CH4}$ versus $\delta^{13}C_{CO2}$) by Milkov and Etiope (2018). These diagrams are based on a

larger geological-geochemical dataset of >20,000 global natural gas samples. Additionally, the isotopic composition of CBG coproduced water is utilized for distinguishing microbial CBG (Golding et al., 2013). In microbial CBG reservoirs, the δD_{H2O} and $\delta^{18}O_{H2O}$ values of CBG coproduced water often plot along or to the left of the global meteoric water line (GMWL), and the $\delta^{13}C$ values of dissolved inorganic carbon (DIC) are often >5‰ (Golding et al., 2013; Chen et al., 2023a). These observations can be interpreted as 1) The CBG coproduced water is mainly from the meteoric water recharge. 2) Methanogens preferentially use isotopically lighter carbon and water-derived isotopically lighter hydrogen to generate methane, leading to ^{2}H enrichment in the residual water and ^{13}C enrichment in CO_2 and DIC (Golding et al., 2013; Chen et al., 2023a,b). However, the isotopic coupling between thermogenic CBG and coproduced water remains poorly constrained.

When distinguishing CBG origins, inconsistencies often remain when applying different indicators (Vinson et al., 2017; Tao et al., 2021). For example, the $\Delta D_{H2O\text{-}CH4}$ ($=\delta D_{H2O}-\delta D_{CH4}$) and $\Delta^{13}C_{CO2\text{-}CH4}$ ($=\delta^{13}C_{CO2}-\delta^{13}C_{CH4}$) indicators respectively suggest that CO_2 reduction and methyl-type fermentation are the dominant methanogenic pathways in the Fuxin Basin CBG (Chen et al., 2023b). In fact, many processes, such as methane oxidation and mixing of thermogenic and secondary microbial gas, can alter the isotopic composition of CBG (Vinson et al., 2017; Tao et al., 2007, 2021). Additionally, isotopic equilibrium and CO_2 dissolution can also significantly affect the isotopic composition of microbial CBG (Turner et al., 2021; Chen et al., 2023a,b). However, there have been few systematic studies of the extent of isotopic equilibrium

and CO_2 dissolution in thermogenic CBG systems (Turner et al., 2021; Chen et al., 2024).

In addition, isotopic reversals of the alkane gases such as $\delta^{13}C_{CH4} > \delta^{13}C_{C2H6} > \delta^{13}C_{C3H8}$, in conventional natural gas, shale gas, and tight sandstone gas have been frequently reported (Dai et al., 2004, 2016; Tilley and Muehlenbachs, 2013; Liu et al., 2018; Milkov et al., 2020). However, there are few reports of isotopic reversals in CBG. To our knowledge, only Faiz et al. (2018) reported isotopic reversals in desorbed coal gases from Australia's Bowen Basin.

To clarify these issues above, we collected CBG and coproduced water samples from highly-mature coalbeds in the Zhuzang syncline, Guizhou, China. In this study, we focus on the origins, CO_2 dissolution, equilibrium and kinetic isotope fractionations, and isotopic reversals of these samples, with discussion on the important implications.

2. Geological setting

The Yanjiao synclinorium (also known as the Bide-Santang Basin) is located in the western part of the Yangtze Continental Block, and mainly consists of the Bide, Shuigonghe, Santang, Agong, and Zhuzang synclines (Fig. 1a) (Li, X. et al., 2016; Ma, 2020). It is one of the important CBG production sites in China. The late Permian Longtan (P_3l) and Changxing (P_3c) formations are the primary coal-bearing strata in the synclinorium (Fig. 1b).

The Zhuzang syncline, located in the east of the Yanjiao synclinorium (Fig. 1a), is an asymmetric syncline. The dip angles of its northwest and southeast limbs are 3–5° and 25–40°, respectively (Li, X. et al., 2016). In the syncline, the coal-bearing P_3l and

P_3c formations, which were deposited in a marine-terrestrial transitional environment, unconformably overlie the Emeishan Basalt ($P_3\beta$) formation, and are overlain by the lower Triassic Feixianguan (T_1f) formation (Li, X. et al., 2016; Liu et al., 2021). The $P_3\beta$ formation and the lower member of T_1f formation act as regional aquitards. There is no hydraulic connection among the P_3l and P_3c aquifers, the $P_3\beta$ formation, and the T_1f formation (Ma, 2020). The hydrodynamic activity is weak in the coal-bearing strata.

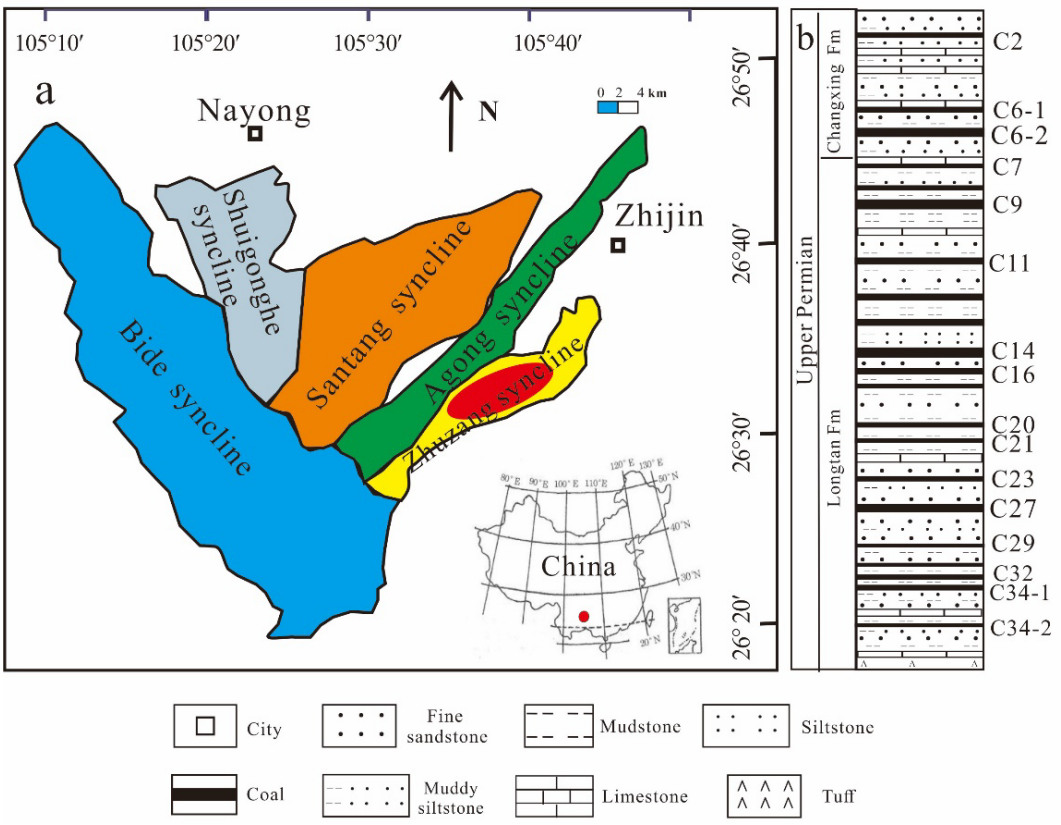

Fig. 1. **(a)** Simplified tectonic map of the Yanjiao synclinorium, Guizhou, China (modified after Zhou et al., 2020 and Li et al., 2022). The red zone in the map of China is the Yanjiao synclinorium. Gas and water samples are collected in the red zone in the Zhuzang syncline. **(b)** Diagram of late Permian coal-bearing strata in the Yanjiao synclinorium (modified after Zhou et al., 2020). Fm = formation.

The coalbeds in the Zhuzang syncline are numerous (> 35 beds), thin (averaging < 4.5 m in thickness), and over mature, with vitrinite reflectance (Ro) values from 2.7% to 4.3% (average 3.4%) (Ma, 2020). The high Ro values are attributed to igneous

intrusion during the Yanshanian orogeny from late Jurassic to early Cretaceous (Liu et al., 2021). The CBG in the Zhuzang syncline mainly formed during the Yanshanian orogeny (Tang et al., 2016). The target coalbeds for CBG recovery mainly include numbers C6, C7, C16, C17, C20, C23, C27 and C30 (see Fig. 1b; Ma, 2020). Their current depths range from 200 to 800 m, which is attributed to coalbed uplift following CBG formation (Meng et al., 2019). The average CBG content exceeds 10 m^3/t (raw basis). Most CBG wells have an average gas production of over 1000 m^3/day/well. Water production ranges from less than 0.5 to more than 5 m^3/day/well. A commingled drainage technique is used for CBG development.

3. Sampling and analytical methods

3.1 Sample collection

Twenty gas and coproduced water samples were collected directly from CBG wellheads in the Zhuzang syncline. The CBG samples were collected in 1L stainless steel cylinders with two valves. The steel cylinder was connected to the CBG well outlet, and the cylinder was flushed with the CBG for 3 mins before sampling by filling up the cylinder. The water samples were filtered by glass fiber filter membranes, and were collected in 300 mL glass bottles with no headspace. The bottles were flushed 3–4 times with CBG coproduced water before sampling.

3.2 Analytical methods

Most of the geochemical data on the samples were measured at the Guangzhou Institute of Geochemistry, Chinese Academy of Sciences. The H-O isotope values of the water samples and the C isotope values of DIC were measured at Beijing LICA United Technology, Ltd.

An Agilent 8890 gas chromatograph (GC) installed with a PoraPLOT Q capillary column (30 m × 0.25 mm × 0.25 μm) was used to measure the molecular composition

of the gas samples. The carrier gas was helium. The GC oven was held at 70°C for 6 mins, then was programmed to increase to 180°C at 15 °C/min, and then was held at 180°C for 4 mins. The relative error was < 0.5%.

The carbon and hydrogen isotopic compositions of the gas samples were measured by gas chromatography-isotope ratio mass spectrometry (GC-IRMS). A 6890N GC installed with a CP-Poraplot Q column (30 m × 0.32 mm × 0.25 μm) was used. The carrier gas was helium. The GC oven was held at 50ºC for 3 mins, then heated to 190ºC at 15 ºC/min, and then held at 190°C for 7 mins. Carbon isotope values were measured using an Isoprime 10 IRMS, and are reported relative to Vienna Pee Dee Belemnite (VPDB) with a precision of ±0.3‰. Hydrogen isotope values were measured using a Trace 1310-Delta V Advantage IRMS, and are reported relative to Vienna Standard Mean Ocean Water (VSMOW) with a precision of ±3‰.

The hydrogen and oxygen isotope values of the water samples were measured by a liquid water isotope analyzer (GLA431-TLWIA), and are reported relative to VSMOW with precision of ±1‰ for hydrogen and ±0.2‰ for oxygen (Chen et al., 2023b). To measure the carbon isotope values of DIC in the water samples, the DIC was converted into CO_2 by treating the water sample with phosphoric acid. The carbon isotope values of the DIC samples were analyzed by a Finnigan MAT 253, and are reported relative to VPDB with precision of ±0.2‰.

The concentrations of total dissolved solids (TDS) in the water samples were calculated by weighing the residues after the water was evaporated to dryness (Chen et al., 2018). The concentrations of major cations (Na^+, K^+, Ca^{2+}, Mg^{2+}, Li^+, NH_4^+) in the water samples were measured by a Metrohm 761 Compact ion chromatograph installed with a Metrosep C4-150/4.0 column. The concentrations of major anions (Cl^-, NO_3^-, SO_4^{2-}, F^-, Br^-) were measured by a Dionex ICS-900 ion chromatograph installed with

an IonPac AS15 column (Chen et al., 2023b). The analytical uncertainties for these ions were better than 5.0%. The bicarbonate (HCO_3^-) concentrations in the water samples were measured by the sulfuric acid (H_2SO_4) titration method using a TitroLine Easy Schott automatic titrator (Chen et al., 2018). A 25 mL water sample was titrated to a pH of 2.5 with a 0.1 mol/L H_2SO_4 solution. Based on the amount of consumed H_2SO_4, the HCO_3^- concentration in the water sample was obtained. The error was < 5%.

4. Results and discussion

4.1 Geochemical composition and origin of the Zhuzang syncline CBG

CH_4, C_2H_6 and CO_2 concentrations in the CBG samples are 97.9–99.5%, 0.02–0.13%, and 0.06–0.83%, respectively (Table 1). The $\delta^{13}C$ values of CH_4 and C_2H_6 in the CBG samples are from -33.4‰ to -31.3‰, and from -35.0‰ to -32.9‰, respectively (Table 2). This suggests that CH_4 and C_2H_6 are thermogenic in origin, because the $\delta^{13}C$ values of thermogenic gases are generally less negative than -50‰ for CH_4 and -45‰ for C_2H_6, whereas those of microbial gases are more negative than these thresholds (Whiticar, 1996; Taylor et al., 2000; Tao et al., 2007). Genetic diagrams of $C_{CH4}/(C_{C2H6}+C_{C3H8})$ versus $\delta^{13}C_{CH4}$ and $\delta^{13}C_{CH4}$ versus δD_{CH4}, combined with an average Ro value of 3.4%, further indicate that the alkane gases in CBG samples are over-mature thermogenic gases (Fig. 2).

In the diagram of $\delta^{13}C_{CH4}$ versus $\delta^{13}C_{CO2}$ (Fig. 3a), isotopic data for the samples fall in the common zone of thermogenic and abiotic gases. However, Fig. 2 shows that CH_4 in the CBG samples is thermogenic. The fractionation factor $\alpha_{CO2\text{-}CH4} = (1000+\delta^{13}C_{CO2})/(1000+\delta^{13}C_{CH4})$ range from 1.021 to 1.026 (Table 2). The low $\alpha_{CO2\text{-}CH4}$ values suggest that CH_4 and CO_2 are thermogenic, because the $\alpha_{CO2\text{-}CH4}$ values of thermogenic gases are usually < 1.03 (Kimura et al., 2010; Chen et al., 2024), however, the $\alpha_{CO2\text{-}CH4}$ values of microbial gases are usually > 1.04 (Whiticar, 1999; Golding et

al., 2013) (Fig. 3b). Hence, CH_4 and CO_2 in the CBG samples are thermogenic in origins.

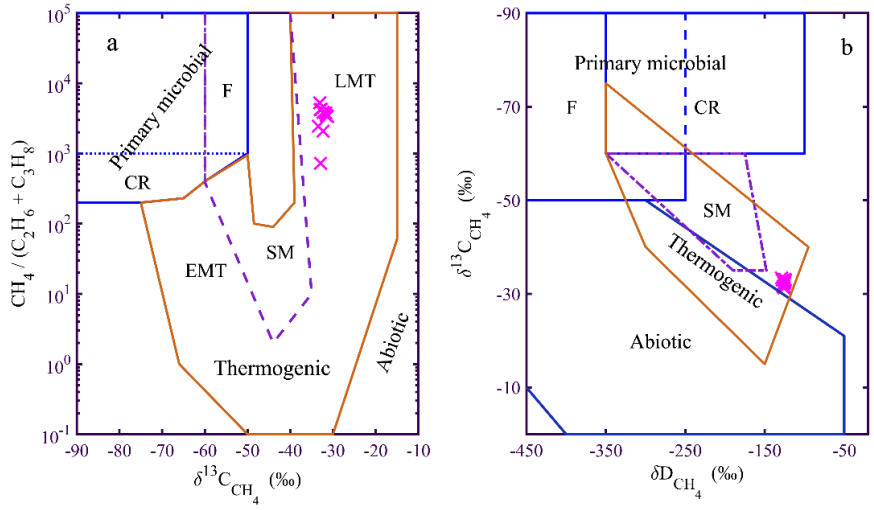

Fig. 2. Genetic diagrams of $C_{CH4}/(C_{C2H6}+C_{C3H8})$ versus $\delta^{13}C_{CH4}$ **(a)**, and $\delta^{13}C_{CH4}$ versus δD_{CH4} **(b)** for coalbed gas samples from the Zhuzang syncline (after Milkov and Etiope, 2018). The diagrams show that the coalbed gas samples are thermogenic gases. F: methyl-type fermentation; CR: CO_2 reduction; SM: secondary microbial; EMT/LMT: early/late mature thermogenic.

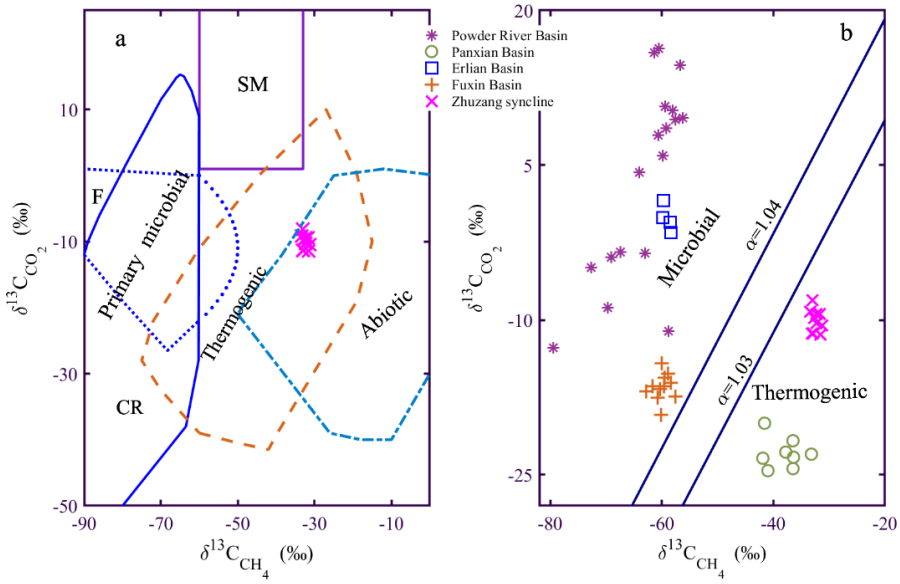

Fig. 3. (a) Genetic diagram of $\delta^{13}C_{CO2}$ versus $\delta^{13}C_{CH4}$ for coalbed gas samples from the Zhuzang syncline (after Milkov and Etiope, 2018). F: methyl-type fermentation; CR:

CO_2 reduction; SM: secondary microbial. **(b)** Plot of $\delta^{13}C_{CH4}$ versus $\delta^{13}C_{CO2}$ for coalbed gas samples from various basins. The coalbed gas from the Powder River Basin (Bates et al., 2011), the Erlian Basin (Chen et al., 2023a), and the Fuxin Basin (Chen et al., 2023b) are microbial gases. The coalbed gas from the Panxian Basin (Tao et al., 2020) are thermogenic gases. The two diagrams show that the gas samples in the Zhuzang syncline are thermogenic gases.

4.2 Geochemical composition and source of CBG coproduced water in the Zhuzang syncline

The CBG coproduced water samples are mainly brackish with total dissolved solids concentrations of 563–6019 mg/L (Table 3). The water samples are significantly enriched in Na^+, HCO_3^- and Cl^-, but are depleted in Ca^{2+}, Mg^{2+} and SO_4^{2-} (Fig. 4). These compositions show that the hydrochemical type of the samples is Na-HCO_3-Cl (Meng et al., 2014).

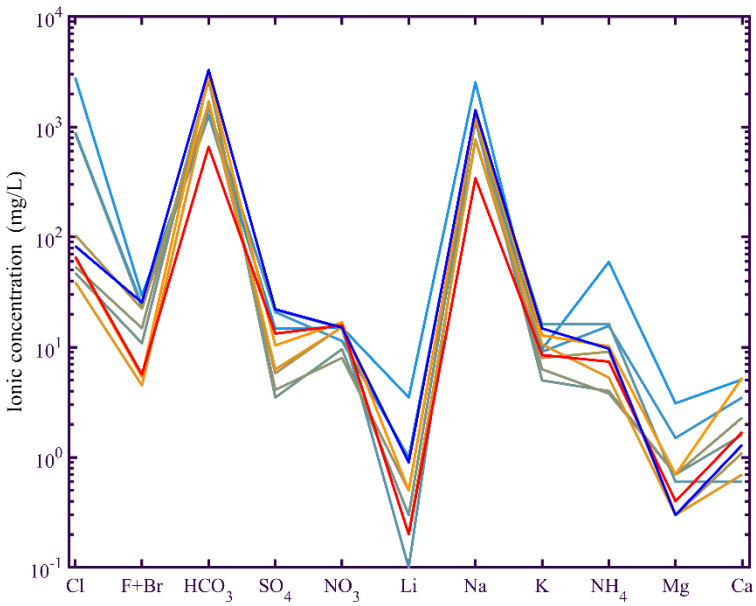

Fig. 4. Schoeller diagram illustrating the chemical compositions of the coalbed gas coproduced water samples in the Zhuzang syncline.

The molar ratios of $[Mg^{2+}+Ca^{2+}]/[HCO_3^-]$ in the water samples range from 0.0008 to 0.006, except for the sample ZJ-3 (0.012). The extremely low ratios not only indicate that HCO_3^- and $(Mg^{2+}+Ca^{2+})$ have different sources but also suggest that extra HCO_3^- promoted the precipitation of Ca^{2+} and Mg^{2+} in the coal-bearing strata of the Zhuzang syncline. Plots using molar ratios (Ca^{2+}/Na^+ versus Mg^{2+}/Na^+ and Ca^{2+}/Na^+ versus HCO_3^-/Na^+; Fig. 5) are important tools in distinguishing the source rocks of Ca^{2+}, Mg^{2+} and HCO_3^- in rivers and groundwater (Gaillardet et al., 1999; Li, Q. et al., 2016; Chen et al., 2023b). However, because of the precipitation of Ca^{2+} and Mg^{2+}, Fig. 5a fails to identify the sources of the Ca^{2+}, Mg^{2+}, and HCO_3^- in the water samples.

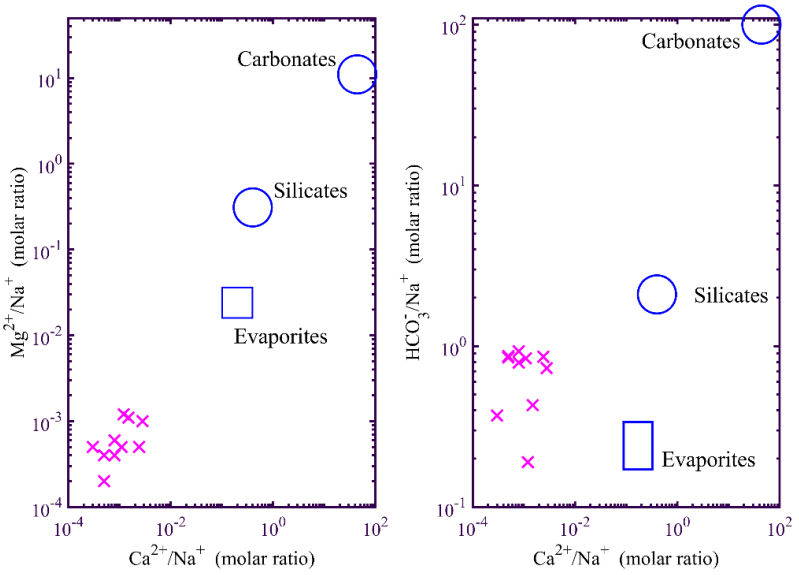

Fig. 5. Plots of molar ratios of Ca^{2+}/Na^+ versus Mg^{2+}/Na^+ **(a)**, and Ca^{2+}/Na^+ versus HCO_3^-/Na^+ **(b)** for CBG samples from the Zhuzang syncline (after Gaillardet et al., 1999 and Li, Q. et al., 2016).

The δD and $\delta^{18}O$ values of the water samples range from -76.3‰ to -40.5‰ and from -10.9‰ to -4.7‰, respectively. The samples (except for sample ZJ-1) plot closely

along the GMWL and the local meteoric water line (LMWL) (Fig. 6). The LMWL equation

$$\delta D_{H2O} = 8.82\delta^{18}O_{H2O} + 22.07 \quad (r^2=0.98) \tag{1}$$

was fitted by Zhu et al. (2014) using precipitation isotopic data from Guiyang station, China. The isotopic distribution characteristics of the water samples (Fig. 6) suggest that the CBG coproduced water in the Zhuzang syncline is mainly from meteoric water recharge.

In addition, Fig. 6a shows that the δD and $\delta^{18}O$ values of CBG coproduced water from various basins plot along the GMWL, regardless of CBG origin. For example, CBG from the Powder River Basin (Bates et al., 2011), the Illinois Basin (Schlegel et al., 2011), the Cesar Rancheria Basin (Castaneda et al., 2022), and the Fuxin Basin (Chen et al., 2023b) is microbial in origin. CBG from the Qinshui Basin (Xu et al., 2016) and the Zhuzang syncline is thermogenic in origin. This characteristic indicates that the source of coalbed water does not reflect the CBG origin.

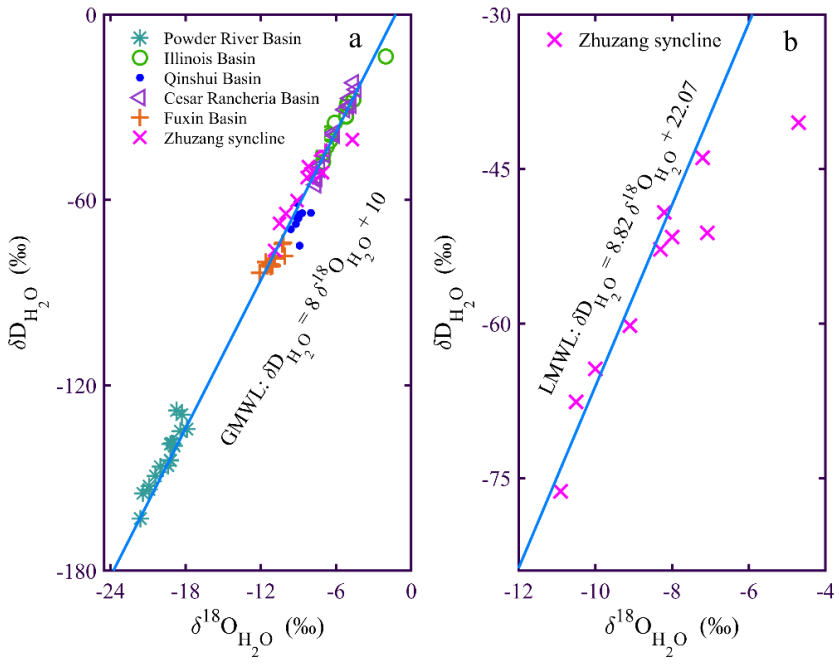

Fig. 6. (a) Plot of δD_{H2O} versus $\delta^{18}O_{H2O}$ for coproduced water samples of coalbed gas from various basins. The samples are from the Powder River Basin (Bates et al., 2011), the Illinois Basin (Schlegel et al., 2011), the Qinshui Basin (Xu et al., 2016), the Cesar Rancheria Basin (Castaneda et al., 2022), the Fuxin Basin (Chen et al., 2023b), and the Zhuzang syncline (This study). **(b)** Expanded plot of δD_{H2O} versus $\delta^{18}O_{H2O}$ for CBG coproduced water samples from the Zhuzang syncline. GMWL: global meteoric water line. LMWL: local meteoric water line.

4.3 Extent of isotopic equilibrium of the gas and water in the Zhuzang syncline

By comparing the apparent isotopic equilibrium temperature with the CBG formation or reservoir temperature, the extent of C and H isotopic equilibrium in the CH_4-C_2H_6-CO_2-HCO_3^--H_2O system in the Zhuzang syncline can be assessed based on the following reactions:

$$^{12}CO_2 + {}^{13}CH_4 \leftrightarrow {}^{13}CO_2 + {}^{12}CH_4 \quad (2)$$

$$H^{12}CO_3^- + {}^{13}CO_2 \leftrightarrow H^{13}CO_3^- + {}^{12}CO_2 \quad (3)$$

$$H^{12}CO_3^- + {}^{13}CH_4 \leftrightarrow H^{13}CO_3^- + {}^{12}CH_4 \quad (4)$$

$$^{12}CO_2 + {}^{13}CH_3 - {}^{12}CH_3 \leftrightarrow {}^{13}CO_2 + {}^{12}CH_3 - {}^{12}CH_3 \quad (5)$$

$$^{13}CH_4 + {}^{12}CH_3 - {}^{12}CH_3 \leftrightarrow {}^{12}CH_4 + {}^{13}CH_3 - {}^{12}CH_3 \quad (6)$$

$$H_2O + CH_3D \leftrightarrow HDO + CH_4 \quad (7)$$

In this study, T_1, T_2, T_3, T_4, T_5, and T_6 denote the apparent equilibrium temperatures of the isotope exchange reactions (2–7), respectively. The calculation methods are described in detail in the Supplementary Material.

The formation temperatures of the CBG samples range from 206°C to 244°C in the Zhuzang syncline (see Supplementary Material). The current reservoir temperatures of CBG are between 25°C and 45°C. For the isotopic exchange reactions (2–5, 7) in the gas and water samples, the apparent equilibrium temperatures T_i (i=1,2,3,4,6) are significantly different from both the formation temperatures and the reservoir temperatures of the CBG samples (Fig. 7, Table 4). Therefore, these reactions (2–5, 7) are in C and H isotopic disequilibrium, both during the CBG formation and in the current reservoirs.

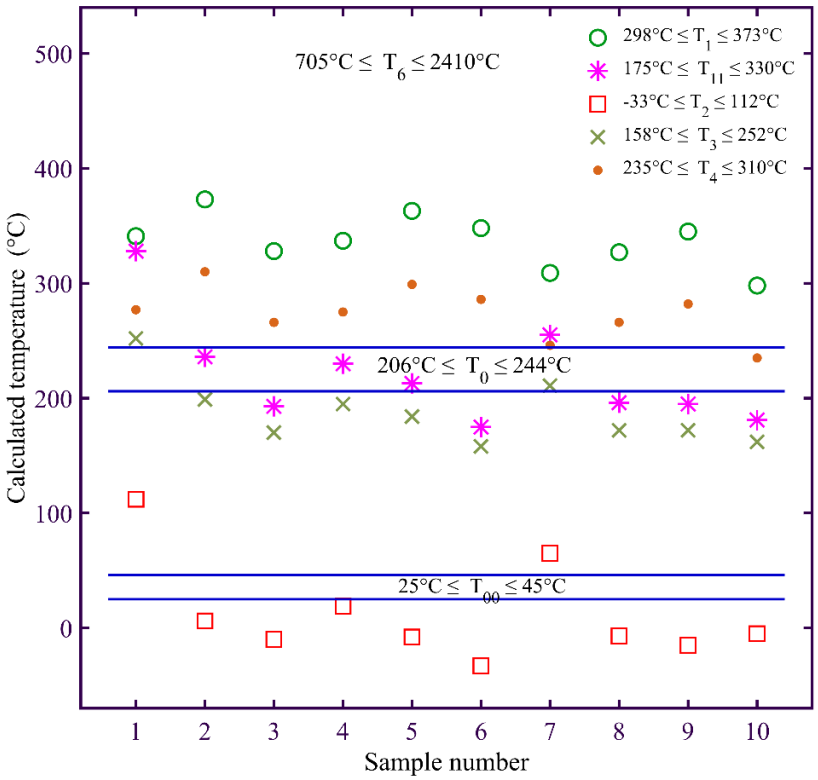

Fig. 7. Comparison of the apparent isotopic equilibrium temperature with the coalbed gas formation or reservoir temperature in the Zhuzang syncline. T_0 and T_{00} denote the formation temperature and the reservoir temperature of the coalbed gas, respectively. T_i (i=1,2,3,4,6) denote the apparent equilibrium temperatures of the isotopic exchange reactions of CH_4-CO_2, CO_2-HCO_3^-, CH_4-HCO_3^-, C_2H_6-CO_2, and CH_4-H_2O. T_{11} denotes

the isotopic equilibrium temperature of the primary CH_4 and CO_2 formed during CBG formation (see text).

The reaction (6) is in equilibrium, the $\Delta^{13}C_{C2H6\text{-}CH4}$ values are greater than 0‰ in the temperature range of 0–400°C (Thiagarajan et al., 2020). The $\Delta^{13}C_{C2H6\text{-}CH4}$ values of all samples are less than 0‰, therefore, the CH_4 and C_2H_6 in the CBG reservoirs are interpreted to be in carbon isotopic disequilibrium.

The carbon isotopic disequilibrium between CH_4 and CO_2 in these samples is mainly attributed to CO_2 dissolution into coalbed water after CBG formation. This process of CO_2 dissolution can lead to more negative $\delta^{13}C_{CO2}$ values, thereby reducing $\Delta^{13}C_{CO2\text{-}CH4}$ values and elevating the apparent isotopic equilibrium temperatures T_1 (Fig. 7). Multiple lines of evidence suggest that most of the primary CO_2 has dissolved into the coal-bearing strata water to become DIC in the Zhuzang syncline. Firstly, coal pyrolysis experiments (Li et al., 2013; Shuai et al., 2018; Li et al., 2018) have shown that coals can produce roughly comparable amounts of CH_4 and CO_2 (Table S1 lists some experiment data). In contrast, field observations of thermogenic CBG and coal-derived gas samples show CH_4/CO_2 ratios significantly greater than 2, often exceeding 20 (Tao et al., 2020; Milkov, 2021; Chen et al., 2024). In the Zhuzang syncline CBG samples, the CH_4/CO_2 ratios are greater than 120 (Table 1). Secondly, the solubility of CO_2 can be more than 5–20 times that of CH_4 under certain conditions (Figs. 8a-b, Table S3). The CO_2/CH_4 solubility ratio increases markedly with decreasing depth under the normal geothermal gradient (30 °C/km) and hydrostatic pressure (10 MPa/km) (Fig. 8c). Dissolved CO_2 in groundwater forms DIC. In this study, the dissolved CH_4

317 concentrations in the coproduced water samples were not measured, making it
318 impossible to estimate the DIC/dissolved CH_4 ratios. However, Owen et al. (2016)
319 reported that the DIC concentrations (primarily from CO_2 dissolution) were often 40
320 times higher than those of dissolved CH_4 in the CBG coproduced water from the Surat-
321 Clarence-Moreton Basin (Fig. 8d). The evidence suggests that less CH_4 and more CO_2
322 can dissolve into the coalbed water during and after coalbed uplift in the Zhuzang
323 syncline. Thirdly, the DIC in the CBG coproduced water samples mainly originates
324 from the dissolution of CO_2 formed during the thermogenic CBG formation rather than
325 alternative sources. In general, the DIC in CBG coproduced water mainly originates
326 from microbial/thermal degradation of coal or carbonate dissolution (Golding et al.,
327 2013). The biodegradation of coal to methane typically results in $\delta^{13}C_{CH4} < -50‰$ and
328 $\delta^{13}C_{DIC} > 5‰$ (Golding et al., 2013; Chen et al., 2023a). However, the $\delta^{13}C_{CH4}$ and
329 $\delta^{13}C_{DIC}$ values of the CBG samples are from -33.4‰ to -31.3‰, and from -9.6‰ to
330 4.4‰, respectively (Table 2). Hence, biodegradation is unlikely to explain the DIC
331 origin. The pH values of the water samples range from 7.91 to 8.73 (Table 3), where
332 HCO_3^- is the dominant DIC component (Myrttinen et al., 2012). Although carbonate
333 dissolution typically results in a molar $[Ca^{2+}]/[HCO_3^-]$ ratio of approximately 1, the
334 observed ratio in these samples is less than 0.006 (Fig. 4b). This discrepancy strongly
335 suggests that carbonate dissolution is not the primary source of DIC (or HCO_3^-).
336 Fourthly, the CBG coproduced water in the Zhuzang syncline is mainly from meteoric
337 water recharge. Meteoric water recharging into coal-bearing strata may supply the
338 necessary volume of water for CO_2 dissolution.

Based on the evidence above, we propose that most of the primary CO_2 generated during the Yanshanian orogeny likely dissolved into coalbed water to become DIC in the Zhuzang syncline. Thus, the $\delta^{13}C$ values of DIC in the CBG coproduced water are nearly equal to those of primary CO_2.

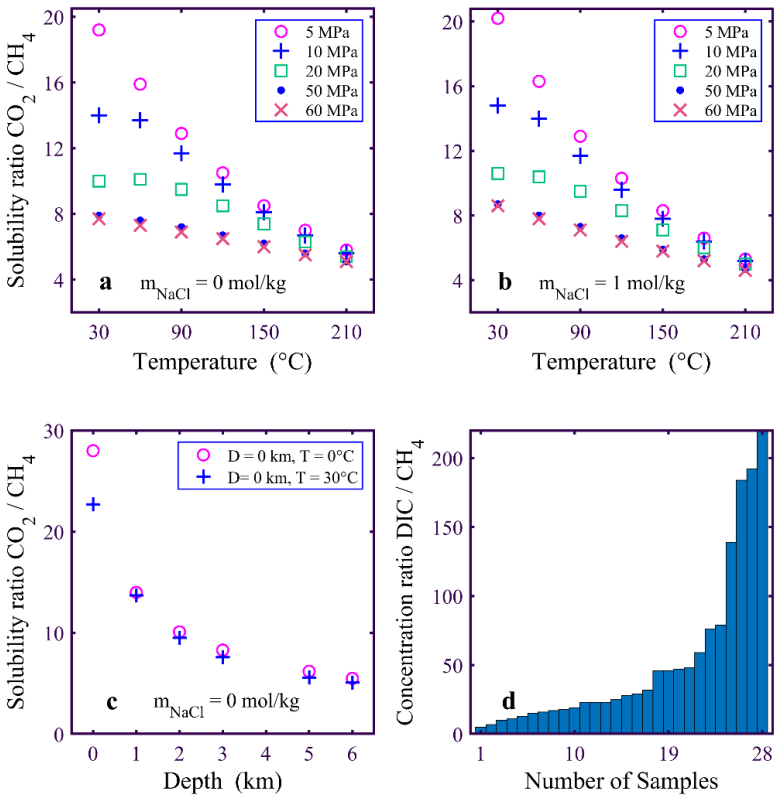

Fig. 8. Comparison of extent of dissolution of CO_2 and CH_4. **(a–b)** Solubility ratios of CO_2 and CH_4 in water under various temperature, pressure and salinity conditions. **(c)** Relationship between the CO_2/CH_4 solubility ratio and depth under normal geothermal gradient and hydrostatic pressure conditions. **(d)** Concentration ratio of DIC and dissolved CH_4 in CBG coproduced water in the Surat-Clarence-Moreton Basin. Solubility data of CO_2 and CH_4 are from Duan and Mao (2006), and Duan and Sun (2003). The concentration data of DIC and CH_4 are from Owen et al. (2016).

We calculated the isotopic equilibrium temperatures (T_{11}) between primary CH_4 and CO_2 using the $\delta^{13}C_{DIC}$ values (as the $\delta^{13}C$ values of primary CO_2) and $\delta^{13}C_{CH4}$ values from the samples. T_{11} ranges from 175°C to 330°C, with an average of 220°C (Table 4). These T_{11} values are consistent with the CBG formation temperature of 206–244°C (average 225°C) (Fig. 7). This suggests that CH_4 and CO_2 were in near carbon isotopic equilibrium during the CBG formation stage.

The maintenance of this near-equilibrium state of primary CH_4 and CO_2 is mainly attributed to two factors. (1) Carbon isotopic exchange between CH_4 and CO_2 proceeds extremely slowly at low temperatures (< 200°C), particularly in the absence of catalysis (Giggenbach, 1982; Stefánsson et al., 2024). (2) After the Zhuzang syncline CBG formation, aside from CO_2 dissolution, other processes, such as CH_4 oxidation, gas mixing, and carbonate mineral precipitation/dissolution, have minimally affected the $\delta^{13}C$ values of the primary CH_4 and CO_2.

Isotopic disequilibrium of CO_2-HCO_3^- in these samples is likely due to CBG recovery. Experimental studies demonstrate rapid carbon isotopic exchange between gaseous CO_2 and DIC species (HCO_3^-, CO_3^{2-}, H_2CO_3 and aqueous CO_2), which achieve equilibrium within hours to days (Mook et al., 1974; Myrttinen et al., 2012). This suggests that CO_2 and HCO_3^- were likely in carbon isotopic equilibrium prior to CBG recovery in the Zhuzang syncline. However, dewatering and fracturing during CBG recovery likely triggered partial CO_2 dissolution or exsolution. This process could significantly alter the $\delta^{13}C$ value of CO_2, given its low concentration in CBG (0.06–0.83%; Table 1). In contrast, the high HCO_3^- concentration in CBG coproduced water

(658.8–3291.6 mg/L; Table 3) would buffer against isotopic shifts, preserving its original $\delta^{13}C$ signature. This differential sensitivity explains the isotopic disequilibrium of CO_2-HCO_3^- in these samples.

The CH_4 and H_2O in these samples are far from hydrogen isotopic equilibrium, as the apparent equilibrium temperatures of 705–2410°C significantly exceed both the CBG formation temperatures (206–244°C) and the reservoir temperatures (25–45°C) (Fig. 7). This large temperature discrepancy suggests that hydrogen isotopic exchange reaction (7) of CH_4-H_2O hardly occurred. Based on the experiment results of Turner et al. (2022), the reaction (7) can occur and reach equilibrium in situ coalbeds on a timescale shorter than millions of years at the temperature above 125°C. However, the reaction (7) cannot occur on a timescale shorter than billions of years at temperatures below 100–125°C without catalysis by methanogens or methanotrophs. In the Zhuzang syncline CBG, the CH_4 is thermogenic in origin. It has not undergone significant oxidation by methanotrophs after the CBG formation. The CBG coproduced water is mainly from late-stage meteoric recharge. Consequently, the isotopic disequilibrium of CH_4-H_2O in the syncline is attributed to the relatively low temperature (< 125°C) during gas-water coexistence and the absence of microbial catalysis.

4.4 Carbon isotope reversals in the Zhuzang syncline CBG

In thermogenic natural gas, alkane gases typically exhibit a normal carbon isotope trend, where $\delta^{13}C_{CH4} < \delta^{13}C_{C2H6} < \delta^{13}C_{C3H8}$ (Dai et al., 2004; Liu et al., 2019). This characteristic is consistent with that of pyrolysis gas derived from kerogen and coal, and conforms with the isotopic fractionation pattern during alkanes formation (Milkov

et al., 2020). Nonetheless, reversed carbon isotope trends, such as $\delta^{13}C_{CH4} > \delta^{13}C_{C2H6} < \delta^{13}C_{C3H8}$ or $\delta^{13}C_{CH4} > \delta^{13}C_{C2H6} > \delta^{13}C_{C3H8}$, in conventional natural gas, shale gas and tight sandstone gas have also been frequently reported (Dai et al., 2016; Milkov et al., 2020). In contrast, such isotopic reversals are rarely observed in CBG (Faiz et al., 2018). In this study, a carbon isotope reversal ($\delta^{13}C_{CH4} > \delta^{13}C_{C2H6}$) was discovered in the Zhuzang syncline CBG samples (Fig. 9).

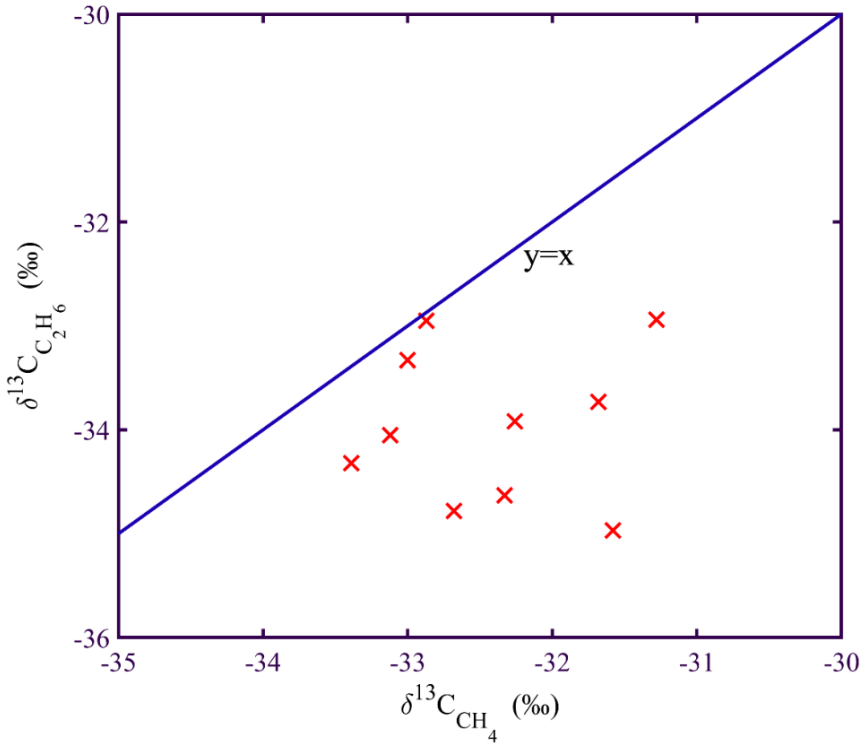

Fig. 9. Plots of $\delta^{13}C_{C2H6}$ versus $\delta^{13}C_{CH4}$ for coalbed gas samples from the Zhuzang syncline. The plot shows that a reversed carbon isotope trend ($\delta^{13}C_{CH4} > \delta^{13}C_{C2H6}$) in the CBG samples.

4.4.1 Reconstructing the $\delta^{13}C$ values of primary ethane in the Zhuzang CBG

We first consider the quantitative changes that could lead to $\delta^{13}C_{CH4} > \delta^{13}C_{C2H6}$ in the CBG samples. Starting from the assumption that $\delta^{13}C_{CH4} < \delta^{13}C_{C2H6}$ in primary CBG, two scenarios are possible: (1) if the $\delta^{13}C_{CH4}$ value decreased or remained unchanged

after CBG formation, for $\delta^{13}C_{CH4}$ to exceed $\delta^{13}C_{C2H6}$, the $\delta^{13}C_{C2H6}$ value must have decreased; (2) if the $\delta^{13}C_{CH4}$ value increased, to achieve $\delta^{13}C_{CH4} > \delta^{13}C_{C2H6}$, the $\delta^{13}C_{C2H6}$ value could have increased, decreased, or remained unchanged.

From Section 4.3, the $\delta^{13}C_{CH4}$ values of the CBG samples did not significantly change after CBG formation. Additionally, according to equation (8)

$$\delta^{13}C_{CH_4} = 8.641\lg(Ro) - 32.8 \quad (8)$$

fitted by Shen and Xu (1991) based on coal-derived gas data, the calculated $\delta^{13}C_{CH4}$ value of the CBG samples is -30.2‰ using the average Ro of 3.4%. The calculated value is consistent with the measured average $\delta^{13}C_{CH4}$ value (-32.3‰) of the CBG samples. Hence, isotope reversals ($\delta^{13}C_{CH4} > \delta^{13}C_{C2H6}$) in the CBG samples indicate a decrease in $\delta^{13}C_{C2H6}$ after CBG formation. In addition, according to statistical results (Dai, 2018; Liu et al., 2019; Tao et al., 2007, 2020), the $\delta^{13}C_{C2H6}$ values of coal-derived gas and thermogenic CBG in China are typically > -28‰. However, the $\delta^{13}C_{C2H6}$ values of our samples are < -28‰ (Fig. 9a), further suggesting a decrease in $\delta^{13}C_{C2H6}$ after CBG formation. In summary, the $\delta^{13}C_{CH4}$ values remained stable after CBG formation, but the $\delta^{13}C_{C2H6}$ values decreased significantly, resulting in $\delta^{13}C_{CH4} > \delta^{13}C_{C2H6}$.

We reconstructed the $\delta^{13}C_{C2H6}$ values of primary ethane under the assumption of carbon isotopic equilibrium of C_2H_6-CO_2 and CH_4-C_2H_6 at the CBG formation temperature range of 206–244°C. This assumption of equilibrium is reasonable. First, CH_4 and CO_2 were in near carbon isotopic equilibrium at the CBG formation stage, suggesting that the CH_4-C_2H_6-CO_2 system was also near carbon isotopic equilibrium. This is supported by their molecular structures. The dissociation energy of the C−H

bond in CH_4 is the highest among alkanes. Moreover, the C−C bonds in C_{2+} alkanes are easy to cleave compared to the C−H bond in CH_4 and the C=O bond in CO_2 (Thiagarajan et al., 2020). Additionally, the equilibrium fractionation factors of C_2H_6-CO_2 and CH_4-C_2H_6 are smaller than those of CH_4-CO_2 under identical thermal conditions, further supporting isotopic equilibrium in the system. Second, some studies have shown that thermogenic natural gases with high thermal maturity (typically Ro > 1.5%) approach carbon and hydrogen isotopic equilibrium at their formation temperatures (Thiagarajan et al., 2020; Xie et al., 2021; Turner et al., 2021). The CBG in the Zhuzang syncline is an over-mature thermogenic gas (2.7–4.3% Ro; Ma, 2020), making it plausible that the CH_4-C_2H_6-CO_2 system attained carbon isotopic equilibrium at their formation temperatures of 206–244°C.

The average CBG formation temperature (225°C) was used as the carbon isotopic equilibrium temperature of C_2H_6-CO_2 and CH_4-C_2H_6. According to the exchange reaction (5) between CH_4 and C_2H_6, the $\delta^{13}C_{C2H6}$ value is calculated as -27.4‰ using the average $\delta^{13}C_{CH4}$ value of the CBG samples (the calculation is described in the Supplementary Material). According to the reaction (4) between C_2H_6 and CO_2, the $\delta^{13}C_{C2H6}$ value is calculated as -25.8‰ using the average $\delta^{13}C_{DIC}$ value of the samples to represent the $\delta^{13}C$ value of the primary CO_2, as most of the primary CO_2 has dissolved into the CBG coproduced water to become DIC (see Section 4.3).

The calculated $\delta^{13}C_{C2H6}$ values (-27.4‰ and -25.8‰) are less negative than the $\delta^{13}C_{CH4}$ values (-33.4‰ to -31.3‰) of the samples and more negative than the $\delta^{13}C_{coal}$ values (typically > -25‰; Xu and Shen, 1990). These characteristics conform to the

isotopic fractionation models of thermogenic CBG formation. Additionally, the calculated $\delta^{13}C_{C2H6}$ values are consistent with those of the majority of China's coal-derived gases, which typically exceed -28‰ (Dai, 2018). These results confirm the reliability of the calculated $\delta^{13}C_{C2H6}$ values.

4.4.2 Explanation of isotope reversals in CBG samples

Various hypotheses for explaining carbon isotope reversals in thermogenic natural gas have been proposed. They include the mixing of gas from different source rocks or different thermal maturities, the mixing with abiotic gases, microbial oxidation, thermochemical sulfate reduction, methane cracking at high temperature, isotopic exchange among alkane gases, decomposition of ethane and propane, and molecular and isotopic fractionation of alkane gases (Xia et al., 2013; Tilley and Muehlenbachs, 2013; Dai et al., 2016; Milkov et al., 2020; Cheng et al., 2020; Xia and Gao, 2024).

Carbon isotope reversals ($\delta^{13}C_{CH4} > \delta^{13}C_{C2H6}$) in the CBG samples cannot be attributed to mixing between gases of different thermal maturities or from distinct source rocks. This is because the CBG in the Zhuzang syncline is an over-mature thermogenic gas, formed as a staged accumulation during the Yanshanian orogeny at temperatures of 206–244°C (see Supplementary Material). The observed $\delta^{13}C_{CH4} > \delta^{13}C_{C2H6}$ in these samples also cannot be attributed to microbial oxidation or thermochemical sulfate reduction. These processes typically result in variable increases in $\delta^{13}C_{CH4}$, $\delta^{13}C_{C2H6}$, CO_2 content or H_2S content in CBG. However, no significant increases in $\delta^{13}C_{CH4}$ or $\delta^{13}C_{C2H6}$ were observed in these samples, and H_2S content was below detection limits. Additionally, based on isotopic equilibrium fractionation

475 principles (Thiagarajan et al., 2020), carbon isotopic exchange among alkane gases
476 cannot lead to $\delta^{13}C_{CH4} > \delta^{13}C_{C2H6}$ in these samples.

477 The observed $\delta^{13}C_{CH4} > \delta^{13}C_{C2H6}$ in the CBG samples cannot be attributed to
478 methane cracking to form ethane. Within the CBG formation temperature range of 206–
479 244°C, ethane is mainly formed through the thermal decomposition of coal and C_{3+}
480 hydrocarbons, rather than via methane cracking (Cesar et al., 2020; Xia and Gao, 2024).
481 Even if methane cracking occurred, the resulting ethane would likely decompose back
482 into methane (Cesar et al., 2020). Based on first-principles calculations, Xia and Gao
483 (2024) proposed that high-temperature (> 200°C) decomposition of ethane and propane
484 could explain the isotopic trend $\delta^{13}C_{CH4} > \delta^{13}C_{C2H6} > \delta^{13}C_{C3H8}$. This model provides a
485 plausible explanation for the isotope reversals observed in Zhuzang CBG. However,
486 experimental validation is required to confirm the theoretical framework.

487 Analyzing approximately 2600 shale gas samples, Milkov et al. (2020) attributed
488 isotope reversals to molecular and isotopic fractionations of alkanes during desorption
489 and diffusion processes within shale formations. As desorption and diffusion of alkanes
490 proceed in shales, the enrichment of residual alkane components increases with
491 molecular mass; however, ^{13}C enrichment in residual alkanes decrease with increasing
492 molecular mass. Consequently, the trend of carbon isotope reversals gradually emerges
493 in shale gas. Milkov et al. (2020) pointed out that $\delta^{13}C_{CH4} > \delta^{13}C_{C2H6}$ in shale gas
494 samples from production wells is often observed when shale rocks exhibit high maturity
495 (Ro > 2%) and significant uplift (> 2km). CBG and Shale gas are both residual gases
496 that remain in source rocks (Milkov et al., 2020). Although the coalbeds in the Zhuzang

497 syncline have high maturity (Ro > 2%) and have experienced significant uplift (> 2 km)
498 since the CBG formation, this reversal mechanism for shale gas does not explain the
499 observed isotope reversals in the CBG samples. According to the mechanism, the
500 $\delta^{13}C_{CH4}$ and $\delta^{13}C_{C2H6}$ values of the CBG samples are expected to increase, and the
501 C_2H_6/CH_4 ratios are also expected to rise. However, the $\delta^{13}C_{C2H6}$ values have decreased
502 since the CBG formation, and the C_2H_6/CH_4 ratios remain very low in the CBG samples
503 (e.g., 0.0002–0.0014; Table 1).

504 We propose that desorption-diffusion processes of alkane gases during CBG
505 recovery lead to $\delta^{13}C_{CH4} > \delta^{13}C_{C2H6}$ in the CBG samples. Alkane gases are typically in
506 an adsorbed state within coalbeds. Compared to ethane, methane has a smaller
507 molecular size and mass, making it easier to desorb and diffuse in coalbeds. During
508 CBG recovery, if production conditions (such as pressure, pore and fracture structure,
509 and pore-throat radius) are favourable for methane desorption and diffusion but
510 unfavourable for ethane, most of the methane but only a portion of the ethane in the in-
511 situ coalbed will desorb and diffuse into CBG wellbores. This process could cause
512 negligible molecular and isotopic fractionation for methane but significant fractionation
513 for ethane. Consequently, compared with in situ CBG, the produced CBG is ethane-
514 depleted and exhibits ethane with ^{13}C depletion, as $^{12}CH_3$-$^{12}CH_3$ desorbs and diffuses
515 faster than $^{13}CH_3$-$^{12}CH_3$. The lower $\delta^{13}C_{C2H6}$ value and the stable $\delta^{13}C_{CH4}$ value may
516 result in $\delta^{13}C_{CH4} > \delta^{13}C_{C2H6}$ in produced CBG.

517 This desorption-diffusion mechanism can explain molecular and isotopic
518 characteristics of methane and ethane in the Zhuzang syncline CBG. The average

519 CH_4/C_2H_6 ratio (3477) of our CBG samples (produced gas) is higher than that (240) of
520 the coal core-desorbed gases (in situ gas) from the exploratory wells in the same area
521 (desorbed gas data from the Sinopec Chongqing Shale Gas Co., Ltd). The $\delta^{13}C_{CH4}$
522 values of produced gas remained stable after CBG formation, whereas the $\delta^{13}C_{C2H6}$
523 values decreased in the Zhuzang syncline. Based on the above assumption, most of
524 methane but only a portion of ethane in situ coalbeds desorb and diffuse into CBG wells
525 during CBG recovery. Consequently, isotopic fractionation of methane is negligible,
526 but significant fractionation occurs in ethane. The relatively slow desorption and
527 diffusion rates of C_2H_6 lead to C_2H_6 depletion in produced CBG. Similarly, due to
528 slower desorption and diffusion rates of ^{13}C-enriched ethane molecules, the $\delta^{13}C_{C2H6}$
529 value of produced gas is lower than that of in situ CBG. The lowered $\delta^{13}C_{C2H6}$ value
530 and the stable $\delta^{13}C_{CH4}$ value result in $\delta^{13}C_{CH4} > \delta^{13}C_{C2H6}$ in the produced CBG samples.
531 This desorption-diffusion mechanism can also explain the similar phenomenon
532 observed in microbial CBG from the Illinois Basin. The $\delta^{13}C_{CH4}$ difference (< 1‰)
533 between produced and in situ CBG from the INS-3 well is insignificant. However, the
534 $CH_4/(C_2H_6+C_3H_8)$ ratio (9385) of produced gas is significantly higher than that (1962)
535 of in situ gas (Strąpoć et al., 2007). The main reason is that CBG recovery caused
536 negligible isotopic fractionation in methane but caused significant compositional
537 fractionation in C_{2+} gases.
538
539 **4.5 Yield ratios of CO_2 and CH_4 formed in the Yanshanian orogeny in the Zhuzang**
540 **syncline**

Knowing the yield ratio of thermogenic CH_4 and CO_2 in coalification is critical for elucidating their formation mechanisms and predicting their emissions to the atmosphere. As discussed in Section 4.3, the CBG in the Zhuzang syncline formed during the Yanshanian orogeny. After the CBG formation, CO_2 dissolution process has significantly affected the $\delta^{13}C$ values of CO_2. However, other processes, such as CH_4 oxidation, gas mixing, and carbonate precipitation/dissolution, have negligible effects on the isotopic compositions of CH_4 and CO_2. Based on the CO_2 dissolution effect, the CO_2/CH_4 yield ratio in the Zhuzang syncline was determined.

In general, coalification has a negligible effect on $\delta^{13}C$ values of coal. For example, the Ro values of the No. 5 coalbed in the Illinois Basin range from 0.63% to 5.31%, but the $\delta^{13}C_{coal}$ values vary only from -25.1‰ to -24.7‰ (Yoksoulian et al., 2016). Moreover, there is no significant positive correlation between them. Whiticar (1996) proposed that the stability of $\delta^{13}C_{coal}$ is due to minimal loss of organic matter during coalification. In contrast, Yoksoulian et al. (2016) suggested that the formation of ^{13}C-depleted CH_4 and ^{13}C-enriched CO_2 maintains the $\delta^{13}C_{coal}$ stability in the Illinois Basin. Pyrolysis experiments indicate that coal can release significant amounts of CH_4 and CO_2 during coalification. For example, coal from the Chuxiong mine (Ro = 0.35%, TOC = 48 wt%) produced a total yield of 661 mg/g TOC of CH_4 and CO_2, with Easy%Ro reaching 3.54% under a heating rate of 1 °C/h. Similarly, coal from the Yilian mine (Ro = 0.53%) yielded 283 mg/g coal of CH_4 and CO_2, with Easy%Ro reaching 4.45% at 2 °C/h (Li et al., 2018). These results indicate that organic matter loss during coalification is not negligible. Hence, as Yoksoulian et al. (2016) suggested, we propose

563 that the formation of ^{13}C-depleted CH_4 and ^{13}C-enriched CO_2 (in both gaseous and
564 dissolved phases) maintains the stability of $\delta^{13}C_{coal}$. Consequently, we use the formulas
565 (9-10):

566 $$f_1 \delta^{13}C_{CO2} + (1 - f_1)\delta^{13}C_{CH_4} \approx \delta^{13}C_{coal} \quad (9)$$

567 $$f_2 \delta^{13}C_{DIC} + (1 - f_2)\delta^{13}C_{CH_4} \approx \delta^{13}C_{coal} \quad (10)$$

568 to estimate the CO_2 percentage ($X_{CO2}/(X_{CO2}+X_{CH4})$) in the CH_4 and CO_2 gases formed
569 during the Yanshanian orogeny in the Zhuzang syncline. The f_1 and f_2 in the formulas
570 (9-10) represent the upper and lower limits of $X_{CO2}/(X_{CO2}+X_{CH4})$ values, respectively.
571 This is because the $\delta^{13}C_{DIC}$ values are greater than the $\delta^{13}C_{CO2}$ values in the samples.

572 Based on the assumption that $\delta^{13}C_{coal}$ = -24.0‰ (Xu and Shen, 1990), the calculated
573 f_1 and f_2 are 34–42% and 22–37%, respectively (Table 5). In general, the lower limits
574 f_2 are closer to the CO_2 percentage in the CH_4 and CO_2 gases formed during the
575 Yanshanian orogeny in the Zhuzang syncline, because most of the primary CO_2 has
576 dissolved into the CBG coproduced water to become DIC.

577 Furthermore, the percentage of dissolved CO_2 in the primary CO_2 (i.e., total gaseous
578 and dissolved CO_2) can be estimated using the equation (11):

579 $$f_3 = 1 - \frac{1/f_2 - 1}{1/m - 1} \quad (11)$$

580 where $m = CO_2/(CH_4+CO_2)$ represents the CO_2 volume fraction in CH_4-CO_2 mixtures
581 in CBG samples.

582 The calculated results show that over 97% of the CO_2 has dissolved into CBG
583 coproduced water in the Zhuzang syncline (Table 5). Additionally, a recent study (Chen
584 et al., 2023a) of microbial CBG from global typical basins also shows that 53–99% CO_2

has dissolved into CBG coproduced water to become DIC. Hence, CO_2 dissolution significantly reduces its content in CBG.

4.6 Implication for CO_2 coalbed storage

Geological storage of CO_2 is a promising approach for reducing greenhouse gas emissions. Subsurface coalbeds are considered important target formations for CO_2 storage (Bashir et al., 2024). Injecting CO_2 into coalbeds can not only store large amounts of CO_2 but also enhance CBG recovery. Furthermore, CO_2 injection into methanogen-bearing coalbeds can significantly increase methanogenesis rates (Tyne et al., 2023).

To evaluate the effectiveness and security of CO_2 coalbed storage, it is essential to understand the mechanisms of CO_2 trapping. CBG, whose predominant component is CH_4, is typically adsorbed onto the surface area of coal pores. Coals have a greater adsorption capacity for CO_2 than for CH_4. Consequently, injecting CO_2 into coalbeds can efficiently displace CH_4 from its adsorption sites (Bashir et al., 2024). Therefore, adsorption trapping plays an important role in CO_2 coalbed storage. However, whether the injected CO_2 remains in a long-term adsorbed state in coalbeds remains unclear.

Coalbeds are typically water-bearing strata. Injecting CO_2 into coalbeds can lead to CO_2-H_2O-rock reactions to form minerals, such as dolomite and siderite (Wang et al., 2016). However, mineral trapping typically proceeds at slow rates. This study of the thermogenic CBG in the Zhuzang syncline, combined with previous research (Chen et al., 2023a) on microbial CBG from global typical basins, shows that 53–99% of post-generation CO_2 has dissolved into CBG coproduced water to form DIC. Tyne et al. (2021) also pointed out that dissolution is responsible for the removal of as much as 74% of the injected CO_2 in the Olla oil field in the USA. Gilfillan et al. (2009) argued that solubility trapping in formation water is the dominant CO_2 sink in natural gas fields.

Hence, we propose that dissolution trapping is an important mechanism for CO_2 storage in coalbeds and other water-bearing strata over geological timescales.

5. Conclusions

The CBG is an over-mature thermogenic gas in the Zhuzang syncline. It formed during the Yanshanian orogeny at temperatures of 206–244℃. The CBG coproduced water is mainly from meteoric water recharge. Its hydrochemical type is Na-HCO_3-Cl.

The CH_4-C_2H_6-CO_2 system is likely in or near carbon isotopic equilibrium during the CBG formation in the Zhuzang syncline. However, later alterations, such as CO_2 dissolution and CBG recovery have broken the equilibrium. A carbon isotope reversal phenomenon ($\delta^{13}C_{CH4} > \delta^{13}C_{C2H6}$) is observed in the CBG samples. After the CBG formation, the $\delta^{13}C_{CH4}$ values remained stable, but the $\delta^{13}C_{C2H6}$ values decreased significantly, resulting in $\delta^{13}C_{CH4} > \delta^{13}C_{C2H6}$. We propose that the CBG recovery processes likely lead to more negative $\delta^{13}C_{C2H6}$ values and thus $\delta^{13}C_{CH4} > \delta^{13}C_{C2H6}$ in the gas samples. The estimated CO_2 percentages in the primary CH_4 and CO_2 gases generated during the Zhuzang CBG formation range from 22% to 37%. However, CO_2 dissolution significantly reduced its content in CBG. This study on thermogenic CBG, combined with prior research on microbial CBG (Chen et al., 2023a), shows that 53–99% of post-generation CO_2 has dissolved into coalbed water to form DIC. Hence, dissolution trapping is an important mechanism for CO_2 coalbed storage over geological timescales.

Author Contributions

Conceptualization: Xiangrui Chen, Yunpeng Wang; Data curation: Xiangrui Chen, Yunpeng Wang, Mingxin Tao; Funding acquisition: Yunpeng Wang, Xiangrui Chen; Investigation: Xiangrui Chen, Meng Wei; Resources: Yunpeng Wang, Meng Wei;

Validation: Yunpeng Wang, Mingxin Tao; Writing – original draft: Xiangrui Chen, Zheng Zhou; Writing – review & editing: All.

Declaration of competing interest

The authors declare that they have no known competing financial interests or personal relationships that could have appeared to influence the work reported in this paper.

Supplementary Material

Supplementary Material is available in the attachment.

Acknowledgments

We thank Kai Bao and Qingguang Li for assistance in sample collection. We thank Qiang Wang, Jian Chen and Jun Li for assistance with sample analyses. Thanks also to SINOPEC Chongqing Shale Gas Co., Ltd. for sampling. This study was funded by the Project of Stable Support for Youth Team in Basic Research Field, CAS (YSBR-017), the China Postdoctoral Science Foundation (2021M703223), the Strategic Priority Research Program of the Chinese Academy of Sciences (XDA14010103), the Project of Theory of Hydrocarbon Enrichment under Multi-Spheric Interactions of the Earth (THEMSIE04010104), and the National Natural Science Foundation of China (42273053). We also thank Simon George from Macquarie University, Australia, for constructive comments and editing of the manuscript.

References

Bashir, A., Ali, M., Patil, S., Aljawad, M.S., Mahmoud, M., Al-Shehri, D., et al., 2024. Comprehensive review of CO_2 geological storage: Exploring principles, mechanisms, and prospects. Earth-Sci. Rev. 249, 104672.

Bates, B.L., McIntosh, J.C., Lohse, K.A., Brooks, P.D., 2011. Influence of groundwater flowpaths, residence times and nutrients on the extent of microbial methanogenesis in coal beds: powder River Basin, USA. Chem. Geol. 284, 45–61.

Castaneda, V.M., Esterle, J.S., Golding, S.D., Gonzalez, S., 2022. Isotopic and hydrogeochemical evidence for biogenic gas in Cuervos Formation coal beds, Cesar Rancheria Basin, Colombia. Int. J. Coal Geol. 249, 103882.

Cesar, J., Nightingale, M., Becker, V., Mayer, B., 2020. Stable carbon isotope systematics of methane, ethane and propane from low-permeability hydrocarbon reservoirs. Chem. Geol, 558, 119907.

Chen, B., Wang, X., Fang, L., Ellam, R.M., Xu, S., 2024. Geochemical evidence for biodegradation in high-rank coals from Qinshui Basin, North China. Org. Geochem. 190, 104755.

Chen, J., Liu, D., Hou, X., Fan, Y., Jia, W., Zhang, B., Xiao, Z., 2018. Origin and evolution of oilfield waters in the Tazhong oilfield, Tarim Basin, China, and their relationship to multiple hydrocarbon charging events. Mar. Petrol. Geol. 98, 554–568.

Chen, X., Tao, M., Zhou, Z., Li, D., 2019. A new theoretical calculation of the equilibrium constant and temperature for the carbon isotope exchange reaction between CH_4 and CO_2. Geothermics 79, 140–144.

Chen, X., Tao, M., Zhou, Z., Holland, G., Wang, Y. 2023a. Geological control on carbon isotope equilibrium and kinetic fractionation of CH_4-CO_2-HCO_3^- in microbial coalbed and shale gas systems. Chem. Geol. 635, 121609.

Chen, X., Wang, Y., Tao, M., Zhou, Z., He, Z., Song, K., 2023b. Tracing the origin and formation mechanisms of coalbed gas from the Fuxin Basin in China using

geochemical and isotopic signatures of the gas and coproduced water. Int. J. Coal Geol. 267, 104185.

Cheng, B., Xu, J., Deng, Q., Liao, Z., Wang, Y., Faboya, O.L., Liu, J., 2020. Methane cracking within shale rocks: A new explanation for carbon isotope reversal of shale gas. Mar. Petrol. Geol. 121, 104591.

Chung, H.M., Gormly, J.R., Squires, R.M., 1988. Origin of gaseous hydrocarbons in subsurface environment: theoretical considerations of carbon isotope distribution. Chem. Geol. 71, 97–104.

Dai, J., 2018. Coal-derived gas theory and its discrimination. Chin Sci Bull, 63, 1291–1305 (in Chinese).

Dai, J., Xia, X., Qin, S., Zhao, J., 2004. Origins of partially reversed alkane $\delta^{13}C$ values for biogenic gases in China. Org. Geochem. 35, 405–41.

Dai, J., Zou, C., Dong, D., Ni, Y., Wu, W., Gong, D., Wang, Y. et al., 2016. Geochemical characteristics of marine and terrestrial shale gas in China. Mar. Petrol. Geol. 76, 444–463.

Duan, Z., Mao, S., 2006. A thermodynamic model for calculating methane solubility, density and gas phase composition of methane-bearing aqueous fluids from 273 to 523 K and from1 to 2000 bar. Geochim. Cosmochim. Acta 70, 3369–3386.

Duan, Z., Sun, R., 2003. An improved model calculating CO_2 solubility in pure water and aqueous NaCl solutions from 273 to 533 K and from 0 to 2000 bar. Chem. Geol. 193, 257–271.

Faiz, M., Zoitsas, A., Altmann, C., Baruch, E., Close, D., 2018. Compositional variations and carbon isotope reversal in coal and shale gas reservoirs of the Bowen and Beetaloo basins, Australia. In: Dowey, P., Osborne, M., Volk, H. (Eds.), Application of Analytical Techniques to Petroleum Systems. Geological Society Special Publications, 484, 20 p.

711 Gaillardet, J., Dupré, B., Louvat, P., Allegre, C. J., 1999. Global silicate weathering and
712 CO_2 consumption rates deduced from the chemistry of large rivers. Chem. Geol.
713 159, 3–30.
714 Giggenbach, W.F., 1982. Carbon-13 exchange between CO_2 and CH_4 under geothermal
715 conditions. Geochim. Cosmochim. Acta 46, 159–165.
716 Gilfillan, S.M., Lollar, B.S., Holland, G., Blagburn, D., Stevens, S., Schoell, M., et al.,
717 2009. Solubility trapping in formation water as dominant CO_2 sink in natural gas
718 fields. Nature 458, 614–618.
719 Golding, S.D., Boreham, C.J., Esterle, J.S., 2013. Stable isotope geochemistry of coal
720 bed and shale gas and related production waters: A review. Int. J. Coal Geol. 120,
721 24–40.
722 Kimura, H., Nashimoto, H., Shimizu, M., Hattori, S., Yamada, K., et al., 2010.
723 Microbial methane production in deep aquifer associated with the accretionary
724 prism in Southwest Japan. The ISME Journal, 4, 531−541.
725 Li, J., Chen, Z., Guo, T., 2022. Practice and understanding of coalbed methane co-
726 production in Zhijin area, Guizhou. Coal Geol. Explor. 50, 163−170 (in Chinese).
727 Li, Q., Ju, Y., Lu, W., Wang, G., Neupane, B., Sun, Y., 2016. Water-rock interaction
728 and methanogenesis in formation water in the southeast Huaibei coalfield, China.
729 Mar. Petrol. Geol. 77, 435–447.
730 Li, W., Zhu, Y. M., Liu, Y., 2018. Gas evolution and isotopic fractionations during
731 pyrolysis on coals of different ranks. Int. J. Coal Geol. 188, 136–144.
732 Li, X., Fu, X., Ge, Y., Chang, X., 2016. Research on sequence stratigraphy,
733 hydrogeological units and commingled drainage associated with coalbed methane
734 production: a case study in Zhuzang syncline of Guizhou province, China.
735 Hydrogeol. J. 24, 2171–2187.
736 Liu, J., Dai, S., Song, H., Nechaev, V. P., French, D., Spiro, B. F., Zhao, J., 2021.
737 Geological factors controlling variations in the mineralogical and elemental

compositions of Late Permian coals from the Zhijin-Nayong Coalfield, western Guizhou, China. Int. J. Coal Geol. 247, 103855.

Liu, Q., Jin, Z., Wang, X., Yi, J., Meng, Q., Wu, X., et al., 2018. Distinguishing kerogen and oil cracked shale gas using H, C-isotopic fractionation of alkane gases. Mar. Pet. Geol. 91, 350–362.

Liu, Q., Wu, X., Wang, X., Jin, Z., Zhu, D., Meng, Q., et al., 2019. Carbon and hydrogen isotopes of methane, ethane, and propane: A review of genetic identification of natural gas. Earth-Sci. Rev. 190, 247–272.

Ma, W., 2020. Study on Geological characteristics of gas reservoir in Zhijin coalbed methane field. China Coalbed Methane, 17, 22–26 (in Chinese).

Meng, M., Wang, Y., Yuan, H., Wang, W., Zhang, H., 2019. Influence factor analysis for coalbed methane production in Zhijin Block. Coal Sci. Technol. 47, 187–192 (in Chinese).

Meng, Y., Tang, D., Xu, H., Li, Y., Gao, L., 2014. Coalbed methane produced water in China: status and environmental issues. Environ. Sci. Pollut. Res. 21, 6964–6974.

Milkov, A. V. 2021. New approaches to distinguish shale-sourced and coal-sourced gases in petroleum systems. Org. Geochem. 158, 104271.

Milkov, A.V., Etiope, G., 2018. Revised genetic diagrams for natural gases based on a global dataset of >20,000 samples. Org. Geochem. 125, 109–120.

Milkov, A.V., Faiz, M., Etiope, G. 2020. Geochemistry of shale gases from around the world: Composition, origins, isotope reversals and rollovers, and implications for the exploration of shale plays. Org. Geochem.143,103997.

Mook, W.G., Bommerson, J.C., Staverman, W.H., 1974. Carbon isotope fractionation between dissolved bicarbonate and gaseous carbon dioxide. Earth Planet. Sci. Lett. 22, 169–176.

763 Myrttinen, A., Becker, V., Barth, J.A.C., 2012. A review of methods used for
764 equilibrium isotope fractionation investigations between dissolved inorganic
765 carbon and CO_2. Earth-Sci Rev.115, 192–199.
766 Owen, D.D.R., Shouakar-Stash, O., Morgenstern, U., Aravena, R., 2016.
767 Thermodynamic and hydrochemical controls on CH_4 in a coal seam gas and
768 overlying alluvial aquifer: New insights into CH_4 origins. Sci. Rep 6, 1–20.
769 Schlegel, M.E., McIntosh, J.C., Bates, B.L., Kirk, M.F., Martini, A.M., 2011.
770 Comparison of fluid geochemistry and microbiology of multiple organic–rich
771 reservoirs in the Illinois Basin, USA: evidence for controls on methanogenesis and
772 microbial transport. Geochim. Cosmochim. Acta 75, 1903–1919.
773 Shen, P., Xu, Y., 1991. The isotopic composition of natural gases from continental
774 sediments in China. Geochem, 22, 144−152 (in Chinese).
775 Shuai, Y., Douglas, P.M., Zhang, S., Stolper, D. A., Ellis, G. S., et al., 2018.
776 Equilibrium and non-equilibrium controls on the abundances of clumped
777 isotopologues of methane during thermogenic formation in laboratory experiments:
778 Implications for the chemistry of pyrolysis and the origins of natural gases.
779 Geochim. Cosmochim. Acta 223, 159–174.
780 Stefánsson, A., Ricci, A., Garnett, M., Gunnarsson-Robin, J., Kleine-Marshall, B.I.,
781 Scott, S.W., et al., 2024. Isotopic and kinetic constraints on methane origins in
782 Icelandic hydrothermal fluids. Geochim. Cosmochim. Acta, 373, 84–97.
783 Strąpoć, D., Mastalerz, M., Eble, C., Schimmelmann, A., 2007. Characterization of
784 the origin of coalbed gases in southeastern Illinois Basin by compound-specific
785 carbon and hydrogen stable isotope ratios. Org. Geochem. 38, 267–287.
786 Tang, S., Tang, D., Xu, H., Tao, S., Li, S., Geng, Y., 2016. Geological mechanisms of
787 the accumulation of coalbed methane induced by hydrothermal fluids in the
788 western Guizhou and eastern Yunnan regions. J. Nat. Gas Sci. Eng. 33, 644–656.

789 Tang, Y., Perry, J.K., Jenden, P.D., Schoell, M., 2000. Mathematical modeling of stable
790 carbon isotope ratios in natural gases. Geochim. Cosmochim. Acta 64, 2673–2687.
791 Tao, M., Chen, X., Li, Z., Ma, Y., Xie, G., Wang, Y., et al., 2021. Variation
792 characteristic and mechanism of carbon isotope composition of coalbed methane
793 under different conditions and its tracing significance. Fuel 302, 121039.
794 Tao, M., Chen, X., Ma, Y., Wang, Y., Li, Z., Xiao, W., Huang, Z., 2020. Geological-
795 geochemical models and isotope fractionation laws and control factors of
796 thermogenic coalbed gas in Panxian, China. Energy Fuel 34, 2665–2673.
797 Tao, M., Shi, B., Li, J., Wang, W., Li, X., Gao, B., 2007. Secondary biological coalbed
798 gas in the Xinji area, Anhui province, China: evidence from the geochemical
799 features and secondary changes. Int. J. Coal Geol. 71, 358–370.
800 Taylor, S.W., Lollar, B.S., Wassenaar, L.I., 2000. Bacteriogenic ethane in near-surface
801 aquifers: Implications for leaking hydrocarbon well bores. Environ. Sci. Technol.
802 34, 4727–4732.
803 Thiagarajan, N., Xie, H., Ponton, C., Kitchen, N., Peterson, B., Lawson, M., Formolo,
804 M., Xiao, Y., Eiler, J., 2020. Isotopic evidence for quasi-equilibrium chemistry in
805 thermally mature natural gases. Proc. Natl. Acad. Sci. USA. 117, 3989–3995.
806 Tilley, B., Muehlenbachs, K., 2013. Isotope reversals and universal stages and trends
807 of gas maturation in sealed, self-contained petroleum systems. Chem. Geol. 339,
808 194–204.
809 Turner, A.C., Korol, R., Eldridge, D.L., Bill, M., Conrad, M., Miller, T.F., Stolper,
810 D.A., 2021. Experimental and theoretical determinations of hydrogen isotopic
811 equilibrium in the system CH_4–H_2–H_2O from 3 to 200°C. Geochim. Cosmochim.
812 Acta 314, 223–269.
813 Turner, A.C., Pester, N.J., Bill, M., Conrad, M.E., Knauss, K.G., Stolper, D.A., 2022.
814 Experimental determination of hydrogen isotope exchange rates between methane

and water under hydrothermal conditions. Geochim. Cosmochim. Acta 329, 231–255.

Tyne, R.L., Barry, P.H., Lawson, M., Byrne, D.J., Warr, O., Xie, H., et al., 2021. Rapid microbial methanogenesis during CO_2 storage in hydrocarbon reservoirs. Nature, 600, 670–674.

Tyne, R.L., Barry, P.H., Lawson, M., Lloyd, K.G., Giovannelli, D., Summers, Z.M., et al., 2023. Identifying and understanding microbial methanogenesis in CO_2 storage. Environ. Sci. Technol, 57, 9459–9473.

Vinson, D.S., Blair, N.E., Martini, A.M., Larter, S., Orem, W.H., McIntosh, J.C., 2017. Microbial methane from in situ biodegradation of coal and shale: A review and reevaluation of hydrogen and carbon isotope signatures. Chem. Geol. 453,128–145.

Wang, K., Xu, T., Wang, F., Tian, H., 2016. Experimental study of CO_2–brine–rock interaction during CO_2 sequestration in deep coal seams. Int. J. Coal Geol. 154, 265–274.

Whiticar, M.J., 1996. Stable isotope geochemistry of coals, humic kerogens and related natural gases. Int. J. Coal. Geol. 32, 191–215.

Whiticar, M.J., 1999. Carbon and hydrogen isotope systematics of bacterial formation and oxidation of methane. Chem. Geol. 161, 291–314.

Whiticar, M.J., Faber, E., Schoell, M., 1986. Biogenic methane formation in marine and freshwater environments: CO_2 reduction vs acetate fermentation–isotope evidence. Geochim. Cosmochim. Acta 50, 693–709.

Xia, X., Chen, J., Braun, R., Tang, Y., 2013. Isotopic reversals with respect to maturity trends due to mixing of primary and secondary products in source rocks. Chem. Geol. 339, 205–212.

Xia, X., Gao, Y., 2024. Compound-specific, intra-molecular, and clumped ^{13}C fractionations in the thermal generation and decomposition of ethane and propane: A DFT and kinetic investigation. Geochim. Cosmochim. Acta 375, 50–63.

Xie, H., Dong, G., Formolo, M., Lawson, M., Liu, J., Cong, F., et al., 2021. The evolution of intra-and inter-molecular isotope equilibria in natural gases with thermal maturation. Geochim. Cosmochim. Acta, 307, 22–41.

Xu, Y., Shen, P., 1990. Isotope geochemistry of fossil fuels of China. Sci. China. 22, 409–418 (in Chinese).

Xu, Z., Liu, Q., Zheng, Q., Cheng, H., Wu, Y., 2016. Isotopic composition and content of coalbed methane production gases and waters in karstic collapse column area, Qinshui Coalfield, China. J. Geochem. Explor. 165, 94–101.

Yoksoulian, L.E., Rimmer, S.M., Rowe, H.D., 2016. Anatomy of an intruded coal, II: effect of contact metamorphism on $\delta^{13}C$ and implications for the release of thermogenic methane, Springfield (no. 5) Coal, Illinois Basin. Int. J. Coal Geol. 158, 129–136.

Zhou, B., Qin, Y., Yang, Z., 2020. Ion composition of produced water from coalbed methane wells in western Guizhou, China, and associated productivity response. Fuel 265, 116939.

Zhu, L., Fan, T., Guo, H., 2014. Sources and stable isotope characteristics of precipitation in southwest of China. Yunnan Geograph. Environ. Res. 26, 61–67 (in Chinese).

Table 1.

Chemical compositions of coalbed gas samples in the Zhuzang syncline.

Sample code	Gas composition (%)						CH_4/CO_2	$CH_4/(C_2H_6+C_3H_8)$
	CH_4	C_2H_6	C_{3-5}	CO_2	N_2	He		
ZJ-1	99.35	0.03	0.003	0.18	0.41	0.03	545	3868
ZJ-2	98.68	0.03	0.001	0.40	0.87	0.02	245	3474
ZJ-3	98.28	0.03	0.061	0.51	1.08	0.04	193	2088
ZJ-4	98.88	0.03	0.004	0.83	0.25	0.02	121	3795
ZJ-5	99.00	0.03	0.001	0.38	0.56	0.03	263	3383
ZJ-6	97.90	0.13	0.006	0.06	1.83	0.07	1686	723
ZJ-7	99.45	0.04	0.002	0.31	0.19	0.01	320	2456
ZJ-8	98.93	0.02	0.001	0.47	0.56	0.02	212	4260
ZJ-9	98.57	0.02	0.002	0.06	1.31	0.04	1531	5277
ZJ-10	98.87	0.02	0.010	0.38	0.70	0.02	260	4238

Table 2.

Isotopic compositions of coalbed gas and coproduced water samples in the Zhuzang syncline.

Sample code	Isotope value (‰)							$\alpha_{CO2-CH4}$	$\Delta^{13}C_{C2-C1}$ [#] (‰)
	$\delta^{13}C_{CH4}$	$\delta^{13}C_{C2H6}$	$\delta^{13}C_{CO2}$	$\delta^{13}C_{DIC}$	δD_{CH4}	δD_{H2O}	$\delta^{18}O_{H2O}$		
ZJ-1	-32.3	-34.6	-10.3	-9.6	-125.6	-40.5	-4.7	1.023	-2.3
ZJ-2	-31.6	-35.0	-11.4	-1.3	-127.1	-43.9	-7.2	1.021	-3.4
ZJ-3	-32.3	-33.9	-9.4	2.8	-124.8	-51.6	-8.0	1.024	-1.7
ZJ-4	-31.7	-33.7	-9.4	-0.8	-126.1	-50.9	-7.0	1.023	-2.1
ZJ-5	-31.3	-32.9	-10.5	1.4	-126.2	-60.2	-9.1	1.021	-1.7
ZJ-6	-32.9	-32.9	-11.3	4.4	-128.2	-67.6	-10.5	1.022	-0.1
ZJ-7	-33.4	-34.3	-9.2	-5.1	-129.1	-49.2	-8.2	1.025	-0.9
ZJ-8	-32.7	-34.8	-9.8	2.0	-124.7	-52.8	-8.3	1.024	-2.1
ZJ-9	-33.1	-34.1	-11.3	1.5	-125.5	-76.3	-10.9	1.023	-0.9
ZJ-10	-33.0	-33.3	-8.1	3.5	-123.6	-64.4	-10.0	1.026	-0.3

[#] $\Delta^{13}C_{C2-C1} = \delta^{13}C_{C2H6} - \delta^{13}C_{CH4}$

Table 3.

Chemical components of coalbed gas coproduced water samples in the Zhuzang syncline.

No.	TDS	pH	Ion concentration (mg/L)											
	mg/L		HCO_3^-	F^-	Cl^-	Br^-	SO_4^{2-}	NO_3^-	Li^+	Na^+	K^+	NH_4^+	Mg^{2+}	Ca^{2+}
ZJ-1	563	7.91	658.8	0.4	66.5	5.3	13.3	15.8	0.2	342.1	8.5	7.4	0.4	1.7
ZJ-2	6019	8.16	1281.0	0.5	2803.0	29.0	14.7	15.1	3.5	2541.6	9.6	59.4	3.1	5.1
ZJ-3	2764	8.22	1488.4	1.8	894.9	22.6	20.8	11.4	1.0	1314.8	9.1	15.6	1.5	3.5
ZJ-4	2706	8.02	1259.0	0.9	876.4	22.2	21.8	14.9	0.1	1268.2	16.1	16.3	0.6	0.6
ZJ-5	2196	8.47	2806.0	4.6	47.3	6.2	3.5	9.6	0.3	1138.1	5.0	4.0	0.7	1.6
ZJ-6	2440	8.66	2693.5	4.7	53.9	10.2	4.1	8.0	0.5	1206.1	6.3	3.8	0.7	2.3
ZJ-7	1464	8.73	1610.4	1.7	104.4	20.7	5.8	15.4	0.2	765.2	8.0	9.1	0.3	1.1
ZJ-8	3126	8.38	3291.6	5.1	82.9	20.4	22.1	15.1	0.9	1420.3	14.8	9.7	0.3	1.3
ZJ-9	1500	8.50	1708.0	4.5	39.0	--	6.3	15.2	0.2	761.2	10.6	5.3	0.3	0.7
ZJ-10	2397	8.47	2891.4	5.4	65.2	--	10.4	16.8	0.5	1267.2	12.8	10.2	0.7	5.3

"--'' denotes data below the measurement limit.

Table 4.

Apparent isotopic equilibrium temperatures of gas and water samples in the Zhuzang syncline*.

Sample code	Temperature (°C)					
	T_1	T_{11}	T_2	T_3	T_4	T_6
ZJ-1	341	330	112	252	277	705
ZJ-2	373	236	6	199	310	748
ZJ-3	328	192	-10	170	266	1050
ZJ-4	337	230	19	195	275	984
ZJ-5	363	213	-8	184	299	1330
ZJ-6	348	175	-33	158	286	1585
ZJ-7	309	257	65	211	246	830
ZJ-8	327	196	-7	172	266	1100
ZJ-9	345	195	-15	172	282	2410
ZJ-10	298	181	-5	162	235	1685

* Gas formation temperatures: 206–244°C; current reservoir temperatures: 25–45°C.
T_1, T_2, T_3 and T_4 are calculated using the $\delta^{13}C$ values of CH_4-CO_2, CO_2-DIC, CH_4-DIC, and C_2H_6-CO_2, respectively. T_6 is calculated using the δD values of CH_4-H_2O. T_{11} is derived using the $\delta^{13}C$ values of the primary CH_4 and CO_2 formed during coalbed gas formation.

881 Table 5.

882 CO_2 content range in primary CH_4 and CO_2 gases, and dissolved CO_2 proportion in

883 total CO_2 in the Zhuzang syncline.

Sample code	$CO_2/(CH_4+CO_2)$ (%)*	$X_{CO2}/(X_{CO2}+X_{CH4})$ (%)#		CO_2 (%)	
		Upper	Lower	Gaseous	Dissolved
ZJ-1	0.18	38	37	0.3	99.7
ZJ-2	0.41	37	25	1.2	98.8
ZJ-3	0.51	36	24	1.7	98.3
ZJ-4	0.83	34	25	2.5	97.5
ZJ-5	0.38	35	22	1.3	98.7
ZJ-6	0.06	41	24	0.2	99.8
ZJ-7	0.31	39	33	0.6	99.4
ZJ-8	0.47	38	25	1.4	98.6
ZJ-9	0.07	42	26	0.2	99.8
ZJ-10	0.38	36	25	1.2	98.8

884 * $CO_2/(CH_4+CO_2)$: CO_2 volume fraction in CH_4-CO_2 mixtures in coalbed gas samples.

885 # Upper and lower limits of CO_2 content in primary CH_4 and CO_2 gases.